OPEN ACCESS
IOP Publishing
Journal of Physics B: Atomic, Molecular and Optical Physics
J. Phys. B: At. Mol. Opt. Phys. **56** (2023) 055502 (13pp)
https://doi.org/10.1088/1361-6455/acb6db

Light–matter quantum interface with continuous pump and probe

Alexander Roth[1], **Klemens Hammerer**[1,*] **and Kirill S Tikhonov**[2]

[1] Institute for Theoretical Physics, Institute for Gravitational Physics (Albert Einstein Institute), Leibniz University Hannover, Callinstraße 38, 30167 Hannover, Germany
[2] St. Petersburg State University, 7/9 Universitetskaya Nab., 199034 St. Petersburg, Russia

E-mail: klemens.hammerer@itp.uni-hannover.de

Received 12 April 2022, revised 12 December 2022
Accepted for publication 27 January 2023
Published 15 February 2023

Abstract

Spin-polarized atomic ensembles probed by light based on the Faraday interaction are a versatile platform for numerous applications in quantum metrology and quantum information processing. Here we consider an ensemble of Alkali atoms that are continuously optically pumped and probed. Due to the collective scattering of photons at large optical depth, the steady state of atoms does not correspond to an uncorrelated tensor-product state, as is usually assumed. We introduce a self-consistent method to approximate the steady state including the pair correlations, taking into account the multilevel structure of atoms. We find and characterize regimes of Raman lasing, akin to the model of a superradiant laser. We determine the spectrum of the collectively scattered photons, which also characterizes the coherence time of the collective spin excitations on top of the stationary correlated mean-field state, as relevant for applications in metrology and quantum information.

Keywords: Faraday interaction, quantum nondemolition, Raman lasing, cumulant expansion, superradiant laser, atomic ensemble, collective scattering

(Some figures may appear in colour only in the online journal)

1. Introduction

Atomic ensembles coupled to light represent a versatile platform for quantum communication [1], for quantum metrology [2], optical atomic clocks [3], and quantum simulations [4]. In particular, the Faraday interaction of light with collective atomic spins has proven to be a powerful tool for realizing a light–matter quantum interface [5], enabling highly efficient quantum control and measurements of atoms [6]. It was used in early quantum optics experiments on quantum non-demolition measurements and has since become a powerful tool for generating spin squeezing of atomic ensembles [7–16]. More generally, the Faraday interaction was also utilized to generate and control exotic many-body entanglement [17, 18]. The exquisite quantum control and long spin coherence time enabled the demonstration of quantum information protocols, including quantum memory and teleportation [19–22] as well as entanglement [23–25] and engineered interactions [26] between remote macroscopic systems. Further quantum technological applications have been demonstrated in entanglement-enhanced magnetometry [27–29] and in quantum back-action-evading measurement of motion [30].

These protocols have commonly been performed in a *pulsed* mode of the external pumping and probing light fields. In this case, the light–matter interaction involves collective spin excitations on top of a fully polarized, uncorrelated spin state [5]. More recently, the regime of *continuous* pumping and probing was explored in a number of experiments and

* Author to whom any correspondence should be addressed.

theoretical investigations. In particular, it has been considered theoretically as a possibility to generate stationary entanglement among remote atomic ensembles [31, 32] and in a hybrid system comprising a mechanical oscillator and a collective atomic spin [33]. Unconditional steady-state entanglement of atomic ensembles achieved in this way has been reported in [24]. Here,—in contrast to the pulsed regime outlined before—optical pumping and probing have to happen at the same time in order to maintain a sufficient stationary atomic polarization. In this regime, the usual assumption of an uncorrelated spin-coherent state becomes a poor approximation for the steady state of atoms. This is due to the fact that at large optical depth, as relevant for an efficient light–matter interface, scattering of photons experiences collective enhancement and introduces strong inter-atomic correlations. The steady state is thus defined from an interplay between the optical pumping of single atoms and the collective scattering of photons induced by the probe field. A systematic theoretical description of a light–matter quantum interface with continuous pump and probe appropriate for this regime is lacking.

Here, we introduce a self-consistent method based on the cumulant expansion to study continuously pumped and probed atomic ensembles beyond standard mean-field theory based on uncorrelated atoms. Our model describes a fairly general setup comprised of an ensemble of Alkali atoms with a ground state spin F subject to continuous optical pumping and transverse probing in a geometry as explored in [19–25]. We give an *ab initio* derivation of an effective Lindblad master equation for an optically thick ensemble of N spin-F systems, accounting for single atom optical pumping as well as collective scattering events generating correlations among atoms. We solve the master equation for its approximate steady state in a cumulant expansion considering two-particle correlations. By means of the quantum regression theorem, we also determine the spectrum of collectively scattered photons. The width of the corresponding spectral lines determines the coherence time of the spin oscillator associated with collective atomic excitation on top of the correlated mean-field state. We find that the system exhibits features of line narrowing and instabilities associated with transitions to regimes of continuous Raman lasing [34, 35]. These effects depend on the optical depth, which sets the strength of collective scattering relative to individual depumping, but also on the geometry of the setup and in particular the angle among the directions of polarization of light and atoms. Such dependencies of line-narrowing on the geometry have been observed experimentally[3].

We develop our treatment of an optically pumped and probed atomic ensemble by drawing a formal analogy to the model of a superradiant laser introduced in [36–38]. Both systems are described by a Lindblad master equation where single atom dynamics competes with cooperative effects described by collective jump operators. In addition, in both cases, this competition encompasses laser transitions which are well accounted for by an improved mean field theory based on cumulant expansions. However, while the superradiant laser is mostly considered on the basis of a two-level approximation, it is crucial to take into account all Zeeman substates and Clebsch–Gordan weights for Raman transitions in order to cover the physics in a continuously pumped and probed atomic ensemble. While a light–matter quantum interface will be operated below the laser threshold, it is still important to understand and characterize the instability provided by the Raman lasing transition. We hope that our study will help to extend the continuous [24, 31–33] or quasi-continuous [7–14] operation of quantum interfaces to higher efficiency and stronger light–matter coupling.

The article is organized as follows. In section 2 we first give a brief introduction to the theory of the superradiant laser and then introduce a slightly more general model, which could be considered a superradiant Raman laser. This model exhibits certain features specific to pumped and probed atomic ensemble, but is simple enough for an analytic characterization of its phase regimes. In section 3 we derive the master equation for a continuously pumped and probed ensemble of Alkali atoms. We discuss its approximate solution based on a cumulant expansion and explore its features on the basis of the model for the generalized superradiant laser. Finally, in section 4 we summarize and give an outlook for future studies.

2. Superradiant laser

2.1. Superradiant laser master equation

In this section, we recapitulate the two-level-system model of the superradiant laser and its most general features, which was treated in great detail in [36–38]. The general setup is shown schematically in figure 1(a). We consider an ensemble of N two-level atoms placed in a cavity with linewidth κ. The cavity frequency ω_c is set to be resonant with the atom transition frequency ω_{eg}, i.e. $\omega_c = \omega_{eg}$. The transition between the ground state $|g\rangle$ and the excited state $|e\rangle$ couples to the cavity mode $\hat{a}$ with a single photon Rabi frequency $\Omega/2$, cf figure 1(b). The system is described by the Lindblad master equation

$$\frac{\mathrm{d}}{\mathrm{d}t}\rho = -i\frac{\omega_{eg}}{2}\left[J^z + \hat{a}^\dagger\hat{a}, \rho\right] - i\frac{\Omega}{2}\left[J^+\hat{a} + J^-\hat{a}^\dagger, \rho\right] + w\sum_{i=1}^{N}\mathcal{D}\left[\sigma_i^+\right]\rho + \kappa\mathcal{D}\left[\hat{a}\right]\rho, \tag{1}$$

where $\mathcal{D}[A]\rho = A\rho A^\dagger - 1/2\left[A^\dagger A, \rho\right]_+$ is a Lindblad superoperator, $J^z = \sum_{i=1}^{N}\sigma_i^z$ and $J^\pm = \sum_{i=1}^{N}\sigma_i^\pm$ are collective spin operators, written in terms of the Pauli operator σ_i^z and the ladder operators $\sigma_i^+ = (\sigma_i^-)^\dagger$ for the ith atom. In addition to the cavity decay, the model takes in an incoherent, non-collective pumping process causing population inversion at an effective rate w. The individual character of pumping is essential, since only in this case the stationary collective polarization of the ensemble will be maintained [39, 40]. This pumping process

[3] We have discussed it with Prof. Eugene Polzik and Prof. Philipp Treutlein.

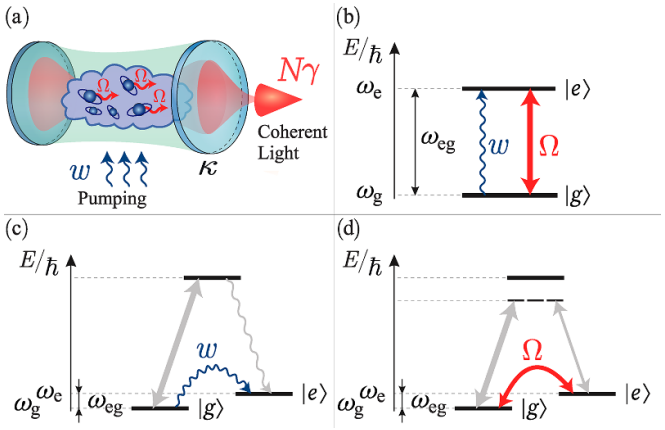

Figure 1. (a) Ensemble of N two-level atoms with single photon Rabi frequency $\Omega/2$ and incoherent pumping rate w, inside a cavity with linewidth κ. The atoms decays through the cavity with rate $\gamma = \Omega^2/\kappa$. (b) Simplified level scheme of the two-level atoms inside the superradiant laser in (a) with coherent atom–cavity interaction (solid arrows) and incoherent pumping rate w (wiggly arrow). (c) Realization of the incoherent pumping process with rate w via a fast-decaying excited state. (d) The coherent coupling of $|g\rangle$ and $|e\rangle$ is achieved through a coherent Λ-type Raman transition.

could correspond e.g. to an additional Λ-type two-photon process involving a laser assisted excitation followed by a spontaneous emission as shown in figure 1(c).

The finite linewidth of the atomic transition could be reflected in an additional Lindblad term in equation (1). However, the physics of the superradiant laser relies in particular on the excited state being long lived on the scale of the cavity decay rate. In this limit spontaneous decay plays a minor role and we choose to suppress it here for the sake of clarity. Its role has been discussed carefully in [36, 39, 41] where long lived transitions in Alkaline earth atoms were considered. Another realization of narrow band transitions can be found in Λ-type Raman transitions as shown in figure 1(d). This corresponds also to the way the first proof-of-principle realizations of superradiant (Raman) lasing have been achieved [38, 42]. We note that the following section will expand on this correspondence, and investigate more complicated two-photon transitions and lasing transitions in multilevel atoms.

In contrast to the conventional laser, the superradiant laser relies on collective effects in the atomic medium to store its coherence, instead of relying on the long coherence time of photons inside the cavity [38]. Therefore, we consider the atomic ensemble coupling to the light field in an extreme bad-cavity regime. In this regime the cavity decay is much faster than all other processes, i.e. $\kappa \gg w, \Omega$, and can be adiabatically eliminated [36], resulting in the permutation invariant master equation, taken here in a frame rotating at the atomic transition frequency ω_{eg},

$$\frac{\mathrm{d}}{\mathrm{d}t}\rho = w\sum_{i=1}^{N}\mathcal{D}\left[\sigma_i^+\right]\rho + \gamma\mathcal{D}\left[J^-\right]\rho \tag{2}$$

with the rate $\gamma = \Omega^2/\kappa$ of the collective decay term.

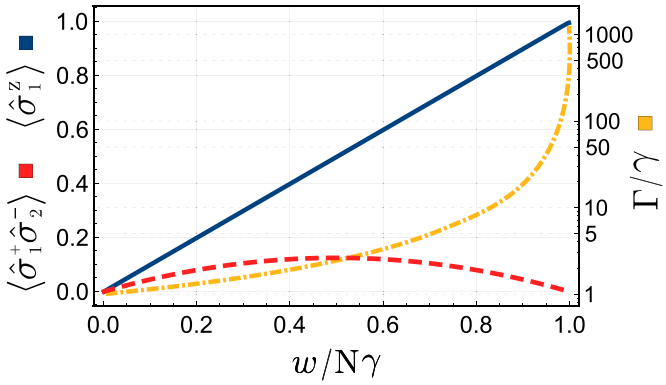

Figure 2. The polarization $\langle\sigma_1^z\rangle$ (blue solid line), two-atom correlations $\langle\sigma_1^+\sigma_2^-\rangle$ (red dashed line) and the dimensionless linewidth Γ/γ (yellow dashed-dotted line) versus dimensionless single-atom pumping rate $w/N\gamma$.

From equation (2) the evolution of the expectation values of $\langle\sigma_1^z\rangle$ and $\langle\sigma_1^+\sigma_2^-\rangle$ follows as

$$\begin{aligned}\frac{\mathrm{d}}{\mathrm{d}t}\langle\sigma_1^z\rangle &= w\left(1-\langle\sigma_1^z\rangle\right) - \gamma\left(1+\langle\sigma_1^z\rangle\right)\\ &\quad - 2(N-1)\gamma\langle\sigma_1^+\sigma_2^-\rangle,\\ \frac{\mathrm{d}}{\mathrm{d}t}\langle\sigma_1^+\hat{\sigma}_2^-\rangle &= \left\{(N-2)\gamma\langle\sigma_1^z\rangle - (w+\gamma)\right\}\langle\sigma_1^+\sigma_2^-\rangle\\ &\quad + \frac{\gamma}{2}\left(\langle\sigma_1^z\rangle+1\right)\langle\sigma_1^z\rangle,\end{aligned} \tag{3}$$

where we used the cumulant expansion and factorized $\langle\sigma_1^+\sigma_2^-\sigma_3^z\rangle = \langle\sigma_1^+\sigma_2^-\rangle\langle\sigma_1^z\rangle$ and $\langle\sigma_1^z\rangle\langle\sigma_2^z\rangle = \langle\sigma_1^z\rangle^2$ due to negligible cumulants $\langle\sigma_1^z\sigma_2^z\rangle_c$ and $\langle\sigma_1^+\sigma_2^-\sigma_3^z\rangle_c$, see [43].

The steady state expectation values can be obtained by setting the left hand sides of the equation (3) to zero and solving the resulting quadratic equation. Figure 2 shows the characteristic linearly increasing polarization $\langle\sigma_1^z\rangle$ (blue solid line) and the inverted parabola of the correlations $\langle\sigma_1^+\sigma_2^-\rangle$ (red dashed line) over the single-atom pumping rate $w/N\gamma$. As one can see, the non-zero two-atom correlations for a large atomic ensemble ($N \gg 1$) corresponding to the superradiant laser regime exist only when the pumping w fulfills the inequalities

$$\gamma < w < N\gamma. \tag{4}$$

At the lower threshold ($w = \gamma$), the pumping overcomes the atomic losses, and the population inversion is established. At the same time, the two-atom correlations build up signifying the onset of superradiance, i.e. atom decay rate γ through the cavity is enhanced by a factor proportional to N (cf figure 1(a)). It is the minimum condition for lasing, which is in contrast to a conventional laser where the threshold is obtained when the pumping overcomes the cavity losses. At the upper threshold ($w = N\gamma$), the two-atom correlations vanish due to the noise imposed by the pumping. Thus, in this case the ensemble consists of random radiators producing thermal light.

The spectrum of light leaving the cavity is $S(\omega) = \mathcal{F}[\langle\hat{a}^\dagger(t)\hat{a}(0)\rangle](\omega) = \frac{\Omega^2}{\kappa^2}\mathcal{F}[\langle J^+(t)J^-(0)\rangle](\omega)$ where $\mathcal{F}$

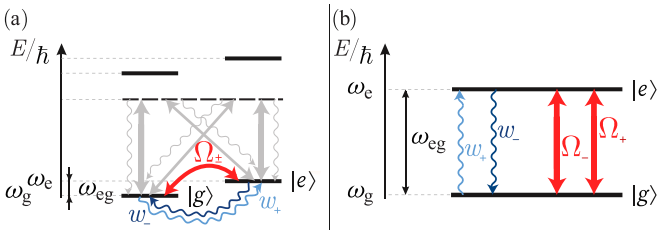

Figure 3. (a) A level scheme of an atom, which has incoherent pumping w_+ (cf figure 1(c)), depumping w_-, and single photon Rabi frequency $\Omega_+/2$ (cf figure 1(d)) and counter rotating rate $\Omega_-/2$. (b) This simplified level scheme shows only the relevant levels and processes of (a). It is effectively the level scheme of figure 1(b) with additional processes for exchanged levels $|g\rangle \leftrightarrow |e\rangle$.

denotes Fourier transform[4]. The equation of motion for the two-time collective dipole correlation function

$$\frac{\mathrm{d}}{\mathrm{d}t}\left\langle J^+(t)J^-(0)\right\rangle = \left(i\omega_{\mathrm{eg}} - \frac{\Gamma}{2}\right)\left\langle J^+(t)J^-(0)\right\rangle \tag{5}$$

with $\Gamma = w + \gamma - (N-1)\gamma\left\langle\sigma_1^z\right\rangle$ follows from the Quantum Regression Theorem [44]. As a result, the spectrum of the output light of the cavity is Lorentzian with a linewidth Γ, which is on the order of γ [36].

At the pumping strength $w_{\mathrm{opt}} = N\gamma/2$ the atom–atom correlations $\left\langle\sigma_1^+\hat{\sigma}_2^-\right\rangle$ reach their maximum, meaning optimal synchronization of the dipole moment of individual atoms and a corresponding maximal collective atomic dipole moment. This results in the maximal intensity and the relatively narrow linewidth of the output laser light [38]. Thus, the superradiant laser regime corresponds to a quite delicate balance between the collective and non-collective processes given in equation (2).

2.2. Generalized superradiant laser master equation

We now consider a generalization of the superradiant laser master equation where we allow for additional processes which can arise in more complicated level schemes such as shown in figure 3(a). These processes correspond to counter-rotating terms in the picture of the effective two-level system, cf figure 3(b), which may still arise as resonant processes from suitable Λ-type transitions. Thus, we consider a Jaynes–Cummings like coupling of each atom to the cavity mode at (effective) single photon Rabi rate Ω_+ and an anti-Jaynes–Cummings type interaction at rate Ω_-. Moreover, we also account for individual pumping at rate w_+ and at individual depumping from the excited to the ground state at rate w_-. All of these processes may arise in double-Λ like transitions as shown in figure 3 and in more complex level schemes as discussed in section 3.

After eliminating the excited states, the master equation that accounts for these additional processes in the effective two-level system corresponds to,

$$\begin{aligned}\frac{\mathrm{d}}{\mathrm{d}t}\rho = &-i\frac{\omega_{\mathrm{eg}}}{2}\left[J^z,\rho\right] - i\left[\left(\frac{\Omega_+}{2}J^+ + \frac{\Omega_-}{2}J^-\right)\hat{a} + h.c.,\ \rho\right]\\ &+ w_+\sum_{i=1}^{N}\mathcal{D}\left[\sigma_i^+\right]\rho + w_-\sum_{i=1}^{N}\mathcal{D}\left[\sigma_i^-\right]\rho + \kappa\mathcal{D}\left[\hat{a}\right]\rho.\end{aligned} \tag{6}$$

Here, ω_{eg} accounts for a (possible) energy difference between the two states which physically corresponds to an energy splitting between the two ground states. Considering the cavity decay as the fastest timescale, i.e. $\kappa \gg \Omega_\pm, w_\pm$, we perform its adiabatic elimination as before, resulting in a field that is slaved to the collective atomic dipole of the atomic ensemble, $\hat{a} \simeq -i(\Omega_+ J_+ + \Omega_- J_-)/\kappa$. The master equation for atoms only becomes

$$\begin{aligned}\frac{\mathrm{d}}{\mathrm{d}t}\rho = &\ w_+\sum_{i=1}^{N}\mathcal{D}\left[\sigma_i^+\right]\rho + \gamma_-\mathcal{D}\left[J^-\right]\rho\\ &+ w_-\sum_{i=1}^{N}\mathcal{D}\left[\sigma_i^-\right]\rho + \gamma_+\mathcal{D}\left[J^+\right]\rho\end{aligned} \tag{7}$$

with rates $\gamma_- = \Omega_-^2/\kappa$ and $\gamma_+ = \Omega_+^2/\kappa$ of the collective terms.

The first two terms are identical to the simplified model of the superradiant laser, which were considered in the previous section, while the third and fourth can be regarded as a superradiant laser with interchanged levels. The model considered here thus is unchanged by relabeling $+ \leftrightarrow -$. We exploit this symmetry here and assume without loss of generality that the single atom pumping generates population inversion in $|e\rangle$, that is $w_+ > w_-$. Furthermore, we are interested in the regime of $w_+, w_- \gg \gamma_-, \gamma_+$ where only collectively enhanced rates $N\gamma_\pm$ are comparable to $w_\pm$.

We proceed as in the previous section, and derive the evolution of expectation values from equation (7)

$$\begin{aligned}\frac{\mathrm{d}}{\mathrm{d}t}\left\langle\sigma_1^z\right\rangle &= w_+\left(1 - \left\langle\sigma_1^z\right\rangle\right) - w_-\left(1 + \left\langle\sigma_1^z\right\rangle\right)\\ &\quad - 2(N-1)\left(\gamma_- - \gamma_+\right)\left\langle\sigma_1^+\sigma_2^-\right\rangle\\ \frac{\mathrm{d}}{\mathrm{d}t}\left\langle\sigma_1^+\sigma_2^-\right\rangle &= \Big\{(N-2)\left(\gamma_- - \gamma_+\right)\left\langle\sigma_1^z\right\rangle\\ &\quad - \left(w_+ + w_- + \gamma_- + \gamma_+\right)\Big\}\left\langle\sigma_1^+\sigma_2^-\right\rangle\\ &\quad + \frac{1}{2}\left(\left(\gamma_- - \gamma_+\right) + \left(\gamma_- + \gamma_+\right)\left\langle\sigma_1^z\right\rangle\right)\left\langle\sigma_1^z\right\rangle,\end{aligned} \tag{8}$$

where we factorized $\left\langle\sigma_1^z\sigma_2^z\right\rangle \approx \left\langle\sigma_1^z\right\rangle^2$ and $\left\langle\sigma_1^+\sigma_2^-\sigma_3^z\right\rangle \approx \left\langle\sigma_1^+\sigma_2^-\right\rangle\left\langle\sigma_1^z\right\rangle$ as in [43] assuming negligible cumulants $\left\langle\sigma_1^z\sigma_2^z\right\rangle_c, \left\langle\sigma_1^+\sigma_2^-\sigma_3^z\right\rangle_c$.

The steady state expectation values can be obtained by setting the left hand sides of equation (8) to zero and solving the resulting quadratic equation. The steady state solution of $\left\langle\sigma_1^+\sigma_2^-\right\rangle$ shows that atom–atom correlations, witnessing the regime of superradiant lasing, exist if and only if the single-atom pumping rate w_+ fulfills the inequality

$$w_+ < N(\gamma_- - \gamma_+)\frac{w_+ - w_-}{w_+ + w_-} - w_-. \tag{9}$$

[4] We use the convention $\mathcal{F}[f(t)](\omega) = \frac{1}{\sqrt{2\pi}}\int_{-\infty}^{+\infty}\mathrm{d}t e^{-\mathrm{i}\omega t}f(t)$.

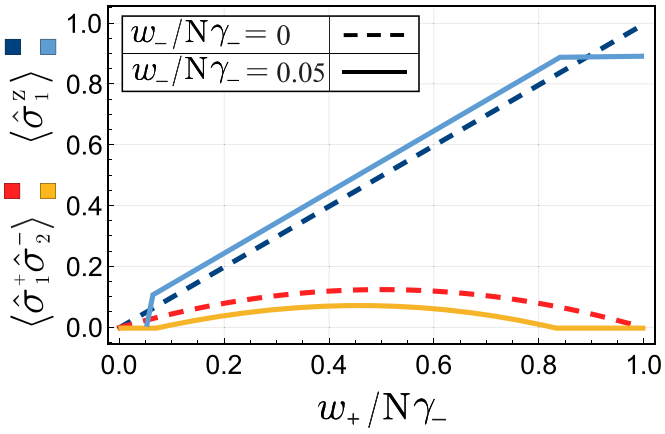

Figure 4. Polarization $\langle \sigma_1^z \rangle$, and atom–atom correlation $\langle \sigma_1^+ \sigma_2^- \rangle$ versus single-atom pump rate w_+, for vanishing collective excitation rate $\gamma_+ = 0$. For comparison, for $w_-/N\gamma_- = 0$ (dashed lines) the curves of figure 2 are reproduced.

Here, we assume the limit of a large atom numbers $N \gg 1$ and restrict equations to leading order in $1/N$. Moreover, we assume strong pumping towards level inversion, $w_+ \gg \gamma_\pm$. In comparison with equation (4), the threshold condition for the generalized superradiance laser has a nonlinear dependence on w_+ for the upper and for the lower bounds. We also recall that we took $w_+ > w_-$ and conclude that a dominant collective emission rate $\gamma_- > \gamma_+$ is necessary for superradiance to occur.

Compared to the model of the superradiant laser, which depended only on the ratio $w/N\gamma$, there are now four independent parameters $N\gamma_\pm$ und $w_\pm$. It will be useful to discuss the steady state physics in terms of the ratios of single atom pumping to collective decay, $w_+/N\gamma_-$, collective excitation to collective decay, γ_+/γ_-, and single atom depumping to collective decay, $w_-/N\gamma_-$.

Figure 4 illustrates the case where $\gamma_+/\gamma_- = 0$, and shows atomic polarization and dipole correlations versus $w_+/N\gamma_-$, in analogy to what was shown for the superradiant laser in figure 2. The overall behavior is similar, but in comparison, the superradiant regime is somewhat reduced for nonzero single atom depumping $w_-/N\gamma_-$ (solid line), as is to be expected. Figure 5 provides a more complete overview, and shows the steady state polarization $\langle \sigma_1^z \rangle$ and atom–atom correlation $\langle \sigma_1^+ \sigma_2^- \rangle$ versus collective excitation rate γ_+/γ_- and individual pumping $w_+/N\gamma_-$. The left (right) column of figure 5 refers to vanishing (nonzero) single atom depumping $w_-/N\gamma_-$. The figure illustrates the superradiant domain and shows that it is excellently characterized by condition (9). Most importantly, figure 5 reveals a rich dependence of the steady state properties on the ratio of collective excitation and decay ratios γ_+/γ_-. Corresponding cuts along this axis are shown in figure 6. The behavior of the system along these will be of importance for our discussion of multilevel atoms in the next section, where we will show that geometrical aspects of the light–matter interactions determine the ratio of the rates

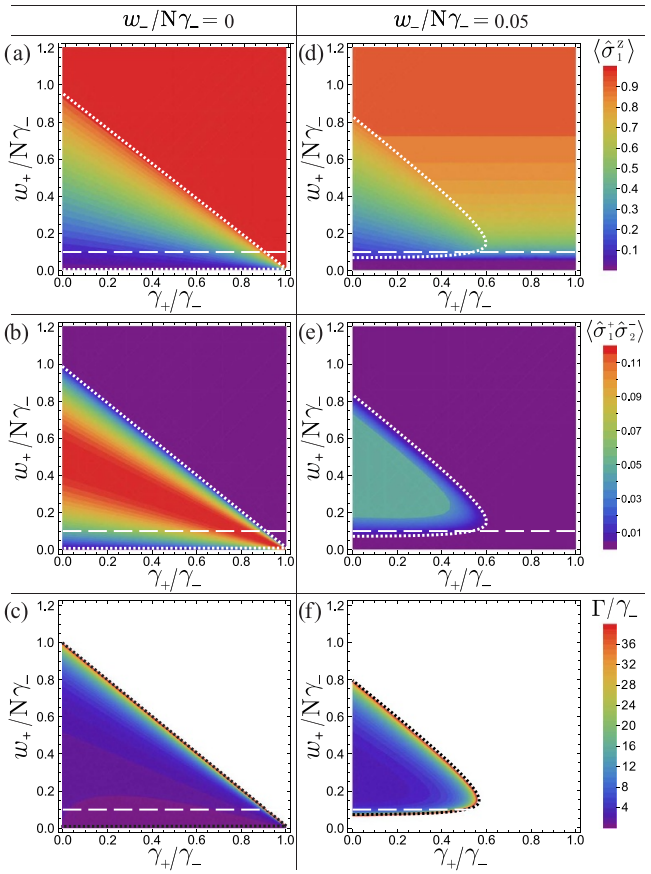

Figure 5. Polarization $\langle \sigma_1^z \rangle$, atom–atom correlation $\langle \sigma_1^+ \sigma_2^- \rangle$, and full-width at half maximum of the Lorentz peak Γ (top to bottom row) versus collective excitation rate γ_+/γ_- and single-atom pump rate $w_+/N\gamma_-$. The single-atom depumping rate is $w_- = 0$ in (a)–(c) and $w_-/N\gamma_- = 0.05$ in (d)–(f). The dashed lines at $w_+/N\gamma_- = 0.1$ correspond to the parameters in in figure 6. The dotted lines are given by equation (9), giving an envelope of the superradiant lasing regime in leading order in $1/N$.

$\Omega_\pm$ and with it the ratio of $\gamma_\pm$. The maximal atom–atom correlations are

$$\max_{w_+} \langle \sigma_1^+ \sigma_2^- \rangle = \frac{1}{8} - \frac{w_-}{N\gamma_+} \frac{1}{\frac{\gamma_-}{\gamma_+} - 1}$$

in leading order in $1/N$, for $\gamma_+ \geqslant \gamma_-$ at the optimal pumping strength $w_{+,\mathrm{opt}} = N(\gamma_- - \gamma_+)/2 - w_-$.

In the generalized superradiant laser the linewidth is still on the order of the atomic linewidth γ_-, even though the ensemble is incoherently pumped with a much stronger rate w_+. We will now show that we essentially have two superradiant lasing transitions, $|e\rangle \to |g\rangle$ and $|g\rangle \to |e\rangle$, radiating at the same time with identical linewidth of the order of γ_-, but different intensities.

As before, the spectrum of the output light $S(\omega) = \mathcal{F}[\langle \hat{a}^\dagger(t)\hat{a}(0)\rangle](\omega) = \frac{\gamma_+}{\kappa}\mathcal{F}[\langle J^+(t)J^-(0)\rangle](\omega) + \frac{\gamma_-}{\kappa}\mathcal{F}[\langle J^-(t)J^+(0)\rangle](\omega)$ is evaluated using the Quantum Regression Theorem [45] based on the equation of motion

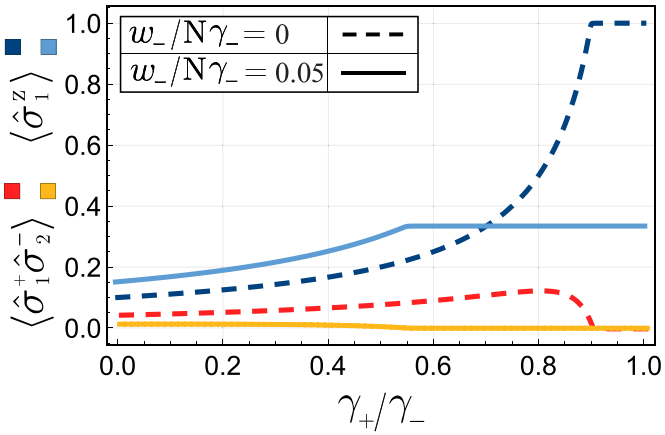

Figure 6. Polarization $\langle \sigma_1^z \rangle$, and atom–atom correlation $\langle \sigma_1^+ \sigma_2^- \rangle$ versus collective excitation rate γ_+/γ_-, corresponding to the dashed lines in figure 5. Varying γ_+ scans through the superradiant regime. For γ_+ close below the upper threshold of the superradiant regime (9), the polarization and atom–atom correlation are strongly dependent on γ_+, and therefore very sensitive to small changes. $w_+/N\gamma_- = 0.1$.

$$\frac{\mathrm{d}}{\mathrm{d}t}\left\langle J^-(t)J^+(0)\right\rangle = \left(-\mathrm{i}\omega_{\mathrm{eg}} - \frac{\Gamma}{2}\right)\left\langle J^-(t)J^+(0)\right\rangle$$

with linewidth $\Gamma = \gamma_- + \gamma_+ + w_+ + w_- - (N-1)(\gamma_- - \gamma_+)\langle\sigma_1^z\rangle$. The corresponding spectrum is given by two Lorentz functions at $\pm\omega_{\mathrm{eg}}$ with heights $S_\pm$ and identical linewidth (full-width at half maximum) Γ. The linewidth Γ for $w_+ > w_-$ to leading order $1/N$ is

$$\frac{\Gamma}{\gamma_-} \approx \frac{W_+ + W_+W_-(W_- - W_+W_- - 1)}{(W_+ - 1)(W_- - 1)W_-}\left(1 - \frac{\gamma_+}{\gamma_-}\right),$$

where we defined the dimensionless variables

$$W_\pm := \frac{(w_+ \pm w_-)(w_+ + w_-)}{N(\gamma_- - \gamma_+)(w_+ - w_-)}.$$

The linewidth Γ is shown in figures 5(c) and (f). We see that the generalized superradiant laser preserves the remarkable feature of the superradiant laser—the linewidth on the order of the effective atomic decay rate γ_-—even for non-vanishing γ_+. And even with additional single-atom depumping rate w_- the linewidth increases only slightly (see figure 5(f)). The spectrum exhibits two asymmetric peaks at the sideband frequencies $\omega = \pm\nu$. The ratio of the sideband intensities $S_\pm$ is given by

$$\frac{S_+}{S_-} = \frac{\gamma_+}{\gamma_-}\frac{1}{1 - \frac{\langle J^z\rangle}{\langle J^+J^-\rangle}} \approx \frac{\gamma_+}{\gamma_-} \tag{10}$$

for $N \gg 1$ in the superradiant regime, which is simply the ratio of collective emission rates at the sidebands. We want to point out that equal Lorentz peak height is not possible, because the superradiant condition (9) cannot be fulfilled for $\gamma_+ = \gamma_-$.

The model of the generalized superradiant laser will be a helpful reference to understand the physics of continuously pumped and probed atomic ensembles, which will be treated in the following.

3. Continuously pumped and probed atomic ensembles

Here, we consider the setup shown in figure 7. An ensemble of Alkali atoms is subject to optical pumping and to continuous, off-resonant probing of spin polarization transverse to the direction of mean polarization. The treatment will closely follow that in [5, 46], but extend it in two aspects: first, instead of pulsed, continuous pump and probe fields will be treated and second, the possibility of collective emissions instead of scattering of independent atoms will be considered. We first develop the corresponding master equation in section 3.1 and then apply it to the examples of atoms with ground state $F = 1$ in section 3.2 and $F = 4$ in section 3.3. These applications will demonstrate the close connection to the model of the generalized superradiant laser introduced in the previous section.

3.1. Master equation of continuously pumped and probed atomic ensembles

We consider N Alkali atoms which are continuously probed by an off-resonant laser of wavelength λ_c propagating in z direction with linear polarization enclosing an angle θ relative to the x-axis, the axis of mean atomic polarization, cf figure 7. The laser couples off-resonantly to one of the atomic D-lines with ground state spin F and excited state spins F'. The respective Zeeman states will be denoted by $|F, m_F\rangle$ and $|F', m_{F'}\rangle$. We assume a spatial distribution of atoms exhibiting a large optical depth $D = \frac{N\sigma_0}{A}$ along the axis of the probe field. Here, $\sigma_0 = \frac{3\lambda^2}{2\pi}$ is the scattering cross section on resonance, and A is the beam cross section. In this limit, the scattering of photons in the z direction occurs in the same spatial mode, which we model here by a cavity mode with linewidth κ to which all atoms couple equally [47]. This (virtual) cavity mode is then adiabatically eliminated in the limit $\kappa \to \infty$, which yields a master equation for the atoms that represents collective emissions in the z direction in free space. Scattering in all other directions is non-collective, and will be covered by suitable Lindblad terms in the master equation. Regarding motion of atom, we will follow the approximations of [5] suitable for treating an ensemble of thermal atoms in a cell. Through thermal averaging, the motion of the atoms is almost decoupled from their spin and the forward-scattered photons.

Our starting point is the master equation for N atoms interacting with the electromagnetic field in dipole approximation. In the electromagnetic field we distinguish the forward scattering modes, which are modeled as a running wave cavity, and all other field modes,

$$\dot{\rho} = \frac{1}{\mathrm{i}\hbar}\left[H_{\mathrm{at}} + H_{\mathrm{cav}} + H_{\mathrm{field}} + H_{\mathrm{int}}, \rho\right] + \kappa\mathcal{D}\left[\hat{a}\right]\rho. \tag{11}$$

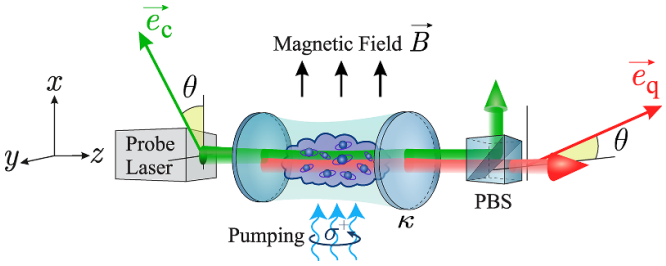

Figure 7. Ensemble of Alkali atoms subject to continuous optical pumping along the direction of a homogeneous magnetic field $\vec{B}$. An off-resonant probe laser propagates along the transverse direction with linear polarization enclosing an angle θ with the mean atomic polarization. At large optical depth, collective emission generates photons in the orthogonal light polarization. PBS denotes a beamsplitter sensitive to polarization used to measure the rotation of the polarization angle of the transmitted probe light.

The Hamiltonians are

$$H_{\rm at} = \hbar \sum_{i=1}^{N} \left\{ \sum_{F',m_{F'}} \omega'_{F',m_{F'}} |F',m_{F'}\rangle\langle F',m_{F'}|_i + \sum_{m_F} \omega_{F,m_F} |F,m_F\rangle\langle F,m_F|_i \right\}$$

$$H_{\rm cav} = \hbar\omega_{\rm c} \hat{a}^\dagger \hat{a}$$

$$H_{\rm field} = \hbar \sum_{\lambda} \int {\rm d}\boldsymbol{k}\, \omega_{\boldsymbol{k}} \hat{a}^\dagger_{\boldsymbol{k},\lambda} \hat{a}_{\boldsymbol{k},\lambda}$$

$$H_{\rm int} = \sum_{i=1}^{N} \sum_{F'} \boldsymbol{E}^-(\boldsymbol{r}_i,t) \boldsymbol{d}^-_{i,FF'} + {\rm h.c.}.$$

We expand the electric field into its coherent ($\mathbb{C}$-number) component, the (quantized) cavity field orthogonally polarized to it, and all other field modes, which are, respectively,

$$\boldsymbol{E}^-(\boldsymbol{r},t) = \boldsymbol{\mathcal{E}}^-(z,t) + \boldsymbol{E}^-_{\rm cav}(z) + \boldsymbol{E}^-_{\rm field}(\boldsymbol{r}), \tag{12}$$

$$\boldsymbol{\mathcal{E}}^-(z,t) = \rho_{\rm c}\sqrt{\Phi} {\rm e}^{-{\rm i}(k_{\rm c} z - \omega_{\rm c} t)} \boldsymbol{e}_{\rm c}, \tag{13}$$

$$\boldsymbol{E}^-_{\rm cav}(z,t) = \rho_q \hat{a}^\dagger {\rm e}^{-{\rm i}k_{\rm c} z} \boldsymbol{e}_{\rm q}, \tag{14}$$

$$\boldsymbol{E}^-_{\rm field}(\boldsymbol{r}) = \sum_{\lambda} \int {\rm d}\boldsymbol{k}\, \rho_\omega \hat{a}^\dagger_{\boldsymbol{k},\lambda} {\rm e}^{-{\rm i}\boldsymbol{k}\boldsymbol{r}} \boldsymbol{e}_{\boldsymbol{k},\lambda}. \tag{15}$$

Here, $\rho_{\rm c} = \sqrt{\frac{\hbar\omega_{\rm c}}{2\epsilon_0 cA}}$, $\rho_{\rm q} = \sqrt{\kappa}\rho_{\rm c}/2$, and $\rho_\omega = \sqrt{\frac{\hbar\omega}{2\epsilon_0(2\pi)^3}}$ is the electrical field per photon for classical, cavity and free field, respectively. $\omega_{\rm c}$ is the laser frequency, $k_{\rm c}$ its wave number, Φ the photon flux, and $\boldsymbol{e}_{\rm c} = (\cos\theta \quad \sin\theta \quad 0)^T$ the linear polarization of the laser field. Regarding the forward scattered quantum field (i.e. the cavity field), $\boldsymbol{e}_{\rm q} = (-\sin\theta \quad \cos\theta \quad 0)^T$ is the linear polarization vector orthogonal to $\boldsymbol{e}_{\rm c}$, and κ the cavity line width. Since we are eventually interested in the free space limit $\kappa \to \infty$, we take the cavity resonance frequency $\omega_{\rm c}$ to be identical to the laser frequency. The dipole operator in $H_{\rm int}$ is expanded as $\boldsymbol{d}_i = \boldsymbol{d}^+_{i,F'F} + \boldsymbol{d}^-_{i,F'F}$ as $\boldsymbol{d}^+_{i,F'F} = \pi_i^{F'} \boldsymbol{d}_i \pi_i^F$, where $\pi_i^F = \sum_{m_F} |F,m_F\rangle\langle F,m_F|_i$ are projectors in the spin-F-subspace of atom i, and $\boldsymbol{d}^-_{i,F'F} = (\boldsymbol{d}^+_{i,F'F})^\dagger$.

In a first step, we consider the dispersive limit of light–matter interaction where the detuning Δ of the laser frequency $\omega_{\rm c}$ from the closest atomic $F \leftrightarrow F'$ transition is large, and only resonant two photon transitions can occur. In this limit, the excited states can be adiabatically eliminated [48]. In the same step, we eliminate the field modes in Born–Markov approximation [49]. This results in a master equation for the ground state spins F and the cavity mode, covering forward scattering of photons,

$$\dot{\rho} = \frac{1}{{\rm i}\hbar}\left[H_{{\rm at},g} + H_{\rm cav} + H^{\rm eff}_{\rm int}, \rho\right] + \kappa \mathcal{D}\left[\hat{a}\right]\rho + \sum_{i=1}^{N}\sum_{\mu=1}^{3} \mathcal{D}\left[L^{\rm eff}_{{\rm at},i,\mu}\right]\rho. \tag{16}$$

From the atomic Hamiltonian $H_{\rm at}$ only the ground state manifold remains,

$$H_{{\rm at},g} := \hbar \sum_{i=1}^{N} \sum_{m_F} \omega_{F,m_F} |F,m_F\rangle\langle F,m_F|_i.$$

Here the effective interaction Hamiltonian for the ground state spins with light is [48]

$$H^{\rm eff}_{\rm int} \approx -\sum_{i=1}^{N} \left(\left(\boldsymbol{E}^-_{\rm cav}(z_i,t)\right)^T \overleftrightarrow{\alpha}_i \boldsymbol{\mathcal{E}}^+(z_i,t) + {\rm h.c.} \right),$$

where we use the polarizability tensor

$$\overleftrightarrow{\alpha}_i := \frac{|d|^2}{\hbar\Delta} \sum_{k=0}^{2} s_k \hat{T}_i^{(k)} \tag{17}$$

with scalar, vector and tensor polarizability operators [50, 51]

$$\hat{T}_i^{(0)} = -\frac{1}{\sqrt{3}} \mathbb{1}_i,$$

$$\hat{T}_i^{(1)} = \frac{\rm i}{\sqrt{2}} \boldsymbol{F}_i \times,$$

$$\hat{T}_i^{(2)} = \frac{1}{2}\left(2\boldsymbol{F}_i \otimes \boldsymbol{F}_i + {\rm i}\boldsymbol{F}_i \times . - \frac{2}{3} (\boldsymbol{F}_i)^2 \mathbb{1}_i \right).$$

d denotes the reduced dipole matrix element (in the convention of [51]), and s_k are dimensionless, real coefficients which depend on the detuning (see (4.43) in [52]). For detunings much larger than the excited states' hyperfine splitting, the tensor polarizability does not contribute, $s_2 \to 0$ [53]. In the effective light matter interaction we keep terms linear in the coherent field, and drop terms which are quadratic in the coherent field (Stark shift of atomic levels) or in the quantum field

(no mean field enhancement). The Stark shift is dropped here for simplicity, but could be easily taken into account in this framework. We note that in the Hamiltonian in equation (17) the atomic coordinates drop out, such that the atomic positions decouple from the dynamics. This is due to the fact that we consider forward scattering only.

The Lindblad terms in the second line of equation (16) account for individual spontaneous emission of each atom. The jump operators can be conveniently labeled in a Cartesian basis with index $\mu = 1,2,3$,

$$L^{\mathrm{eff}}_{\mathrm{at},i,\mu} \approx \sqrt{\gamma'}\left(\overleftrightarrow{\alpha}_i \boldsymbol{\mathcal{E}}^+\right)_\mu ,$$

where we define $\gamma' = \frac{\omega_c^3}{6\pi\hbar\epsilon_0 c^3}$. We note that, due to the structure of Lindblad terms, the second line of equation (16) is actually basis independent. A convenient choice will be to use $\{\boldsymbol{e}_c, \boldsymbol{e}_q, \boldsymbol{e}_z\}$.

In the next step we eliminate the cavity field in the free space limit based on the methods of [45, 49]. The resulting master equation, written in a rotating frame with respect to $H_{\mathrm{at},g}$, in the limit $\kappa \to \infty$ is

$$\dot{\rho} = \sum_\omega \left\{ \gamma_{\mathrm{dec}} \sum_{i=1}^N \sum_{\mu=c,q,z} \mathcal{D}\left[V_i^\mu(\omega)\right]\rho + \gamma\, \mathcal{D}\left[V^q(\omega)\right]\rho \right\} + w\sum_{i=1}^N \mathcal{D}\left[F_i^+\right]\rho. \tag{18}$$

We introduce here the dimensionless jump operators

$$V^{\mathrm{q}}(\omega) = \sum_{i=1}^N V_i^{\mathrm{q}}(\omega), \tag{19}$$

$$V_i^\mu(\omega) = \sum_{\substack{m_F,m_F' \\ \omega_{m_F}-\omega_{m_F'}=\omega}} |m_F\rangle\langle m_F|V_i^\mu|m_F'\rangle\langle m_F'| \tag{20}$$

for atom i for $\mu \in \{\mathrm{c},\mathrm{q},\mathrm{z}\}$. The sum is over all pairs (m_F, m_F') with a given energy splitting $\hbar\omega = \hbar(\omega_{m_F} - \omega_{m_F'})$, and

$$V_i^\mu := \sum_{k=0}^2 s_k \boldsymbol{e}_\mu^T \hat{T}_i^{(k)} \boldsymbol{e}_c. \tag{21}$$

In equation (18) we introduced the *decoherence rate due to spontaneous emission*,

$$\gamma_{\mathrm{dec}} = \Phi\gamma'\left(\frac{|d|^2}{\hbar\Delta}\rho_c\right)^2 = \frac{\Phi}{8}\frac{\sigma_0}{A}\left(\frac{\gamma_0}{\Delta}\right)^2,$$

and the *rate of collective forward scattering*,

$$\gamma = \Phi\left(\frac{\omega_c|d|^2}{2\epsilon_0 cA\hbar\Delta}\right)^2 = \frac{\Phi}{16}\left(\frac{\sigma_0}{A}\right)^2\left(\frac{\gamma_0}{\Delta}\right)^2. \tag{22}$$

We use here the spontaneous emission rate $\gamma_0 = \frac{\omega_c^3|d|^2}{3\pi\epsilon_0\hbar c^3}$. We note that due to the collective nature of the jump term associated with collective scattering, the effective rate of these processes is $N\gamma$. Therefore, the relative strength of collective scattering with respect to decoherence due to spontaneous emission, $\frac{N\gamma}{\gamma_{\mathrm{dec}}} = \frac{D}{2}$, becomes large for sufficiently large optical depth.

Furthermore, we add in the last line of equation (18) a Lindblad term accounting for optical pumping to the ground state with $m_F = F$. As explained earlier, we employ a phenomenological description for this process, as our main aim here is to provide a microscopic picture for the non-collective and collective effects of the continuous probe. The microscopic theory of optical pumping is of course well established, and can in principle be used to give a more realistic account than the minimal model used here. The master equation (18) is the main result of this section. For more details on its derivation we refer to [52].

It is instructive to consider in more detail the form of the jump operator in equation (21)

$$V_i^{\mathrm{q}} = \mathrm{i}\frac{s_1}{2}\left(F_i^- - F_i^+\right) - s_2\left(\frac{\mathrm{i}\cos(2\theta)}{\sqrt{2}}W_1 + \frac{\sin(2\theta)}{4}W_2\right) \tag{23}$$

occurring in the collective jump term in equation (18), where we defined the operators

$$W_1 := \left(F_i^0 + \frac{1}{2}\right)F_i^- + \left(F_i^0 - \frac{1}{2}\right)F_i^+,$$

$$W_2 := 3\left(F_i^0\right)^2 - (\boldsymbol{F}_i)^2 + \left(F_i^-\right)^2 + \left(F_i^+\right)^2.$$

The operator W_1 collects processes which change m by ± 1, and W_2 contains changes by 0 or ± 2. We emphasize that the θ-dependence is an effect of the tensor component $\hat{T}^{(2)}$ in the polarizability tensor, and scales with $s_2 \ll s_1$ for large detuning.

While both W_1 and W_2 can be considered as corrections to the dominant dynamics provided by the vector polarizability, their impact on the dynamics is very different: W_1 corrects the dominant ± 1 transitions in the vector polarizability, which contributes crucially to the unbalancing of transition rates among the Zeeman states responsible for the lasing behavior, as will be discussed below. In contrast, the ± 2 transitions added by W_2 are comparatively slow, and make a negligible contribution to the dynamics. Therefore, we will disregard them below in our analytical considerations, but include them in the numerical analysis only.

3.2. Ground-state spin $F = 1$

We will now evaluate the master equation in equation (18) for the case of spin $F = 1$. In order to highlight the most important features more clearly, we deliberately omit the W_2 components in the jump operators in equation (23) for now. With this simplification, the master equation becomes

$$\dot{\rho} = \frac{1}{i}\sum_{i=1}^{N}\left[\sum_{m=-1}^{1}\omega_m|m\rangle\langle m|_i,\rho\right] + \gamma\mathcal{D}\left[V^+(\theta)\right]\rho + \gamma\mathcal{D}\left[V^-(\theta)\right]\rho + w_+\sum_{i=1}^{N}\mathcal{D}\left[F_i^+\right]\rho + w_-\sum_{i=1}^{N}\mathcal{D}\left[F_i^-\right]\rho. \quad (24)$$

Here, the first term on the right hand side accounts for the splitting of the levels $|m\rangle$ in the external magnetic field with Zeeman energies ω_m where now $m=-1,0,1$. The terms in the second line represent the effect of collective scattering of photons in the z-direction. The collective jump operators depend on the angle θ between the polarizations of atoms and light, and are given by

$$V^{\pm}(\theta) = \sum_{i=1}^{N} V_i^{\pm}(\theta) \quad (25)$$

with single atom operators

$$V_i^{\pm}(\theta) = s_1\left(1+\epsilon\cos(2\theta)\left(\mp F_i^0 + \mathbb{1}/2\right)\right)F_i^{\pm}. \quad (26)$$

We define $\epsilon = \sqrt{2}\,|s_2/s_1|$ measuring the relative weight of the ground states' tensor to vector polarizability. In the limit of large detuning ϵ vanishes asymptotically. The terms in the last line describe individual optical pumping and depumping at rate $w_\pm$, respectively. As in the case of the generalized superradiant laser in section 2.2, we restrict the analysis to $w_+ > w_-$. The collective jump operators are associated with transitions between Zeeman states $|n\rangle$ to $|m\rangle$ where $\Delta m = m-n = \pm 1$ for $V^{\pm}(\theta)$, respectively. It will be useful to define the single-atom transition rates for these transitions

$$\gamma_{m,n} = \gamma\left|\langle m|V_i^{m-n}(\theta)|n\rangle\right|^2 = \gamma s_1\left(1+\epsilon\cos(2\theta)\left(\mp m + 1/2\right)\right)^2. \quad (27)$$

It can be seen that the angle θ controls the balance between $\Delta m = \pm 1$ transitions. Figure 8(a) illustrates how the relative weight of $\gamma_{0,\pm1}$ and $\gamma_{\pm1,0}$ shifts with θ. From the discussion of the generalized superradiant laser model in section 2.2, it should be expected that the relative weight crucially determines the regimes of superradiance, as shown schematically in figure 8(b).

As in the previous sections, the master equation (24) is solved for the steady state in a cumulant expansion. For this purpose, the master equation is expanded in an operator basis (with elements A_i^{α} for particle i), and three-particle correlators are approximated as $\langle A_1^{\alpha_1}A_2^{\alpha_2}A_3^{\alpha_3}\rangle \approx \langle A_1^{\alpha_1}A_2^{\alpha_2}\rangle\langle A_3^{\alpha_3}\rangle + \langle A_1^{\alpha_1}A_3^{\alpha_3}\rangle\langle A_2^{\alpha_2}\rangle + \langle A_2^{\alpha_2}A_3^{\alpha_3}\rangle\langle A_1^{\alpha_1}\rangle - 2\langle A_1^{\alpha_1}\rangle\langle A_2^{\alpha_2}\rangle\langle A_3^{\alpha_3}\rangle$. From this approximate solution we can extract information on single particle observables such as level populations and mean polarization, as well as on the magnitude of two-particle correlations. The latter we quantify by the norm $\|\tau_2\|_2$ of $\tau_2 = \rho_2 - \rho_1\otimes\rho_1$, where ρ_n denotes the n-body reduced density operator. The dependence of these quantities on the angle θ are shown in figures 9 and 10.

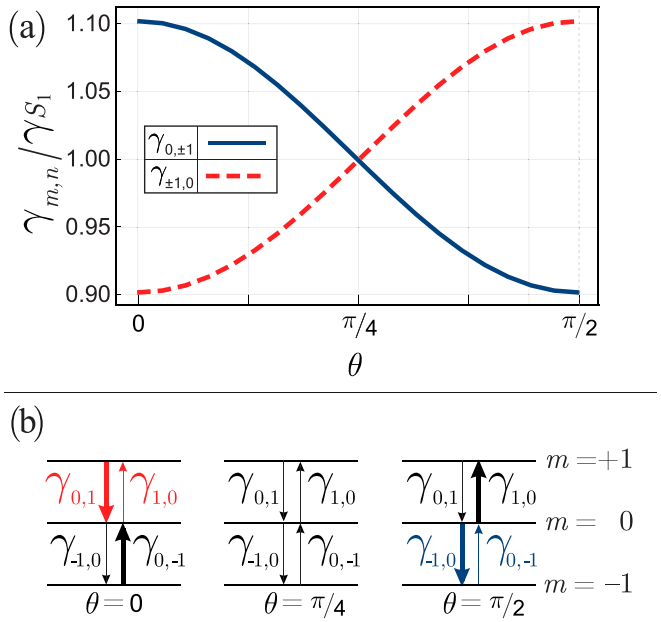

Figure 8. (a) Transition rates $\gamma_{m,n}$ versus angle θ, for a relative weight of tensor to vector polarizability $\epsilon = 0.1$. Rates of transitions in opposite direction and involving different levels are identical, i.e. $\gamma_{0,1} = \gamma_{0,-1}$ and $\gamma_{-1,0} = \gamma_{1,0}$. (b) Transition rates $\gamma_{m,n}$ between the different ground state levels m for angles $\theta = 0, \pi/4, \pi/2$. The thickness of the line represents a measure for the transition strength. Transition fulfilling the conditions for superradiant lasing are shown in red and blue.

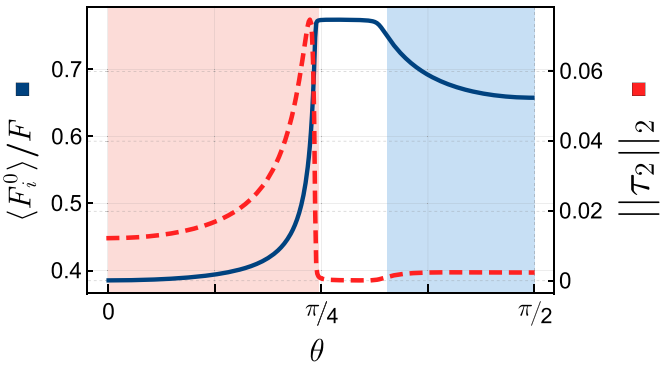

Figure 9. Polarization $\langle F_i^0\rangle/F$, and norm of two-atom correlations $\|\tau_2\|_2$ over the angle θ, where $\tau_2 := \rho_2 - \rho_1\otimes\rho_1$ and ρ_n is the reduced density matrix of n atoms. Red and blue shaded regions correspond to $\|\tau_2\|_2 > 10^{-3}$ indicating significant two-atom correlations and associated lasing. The parameters are chosen the following way: for a fixed $N\gamma$ and $N = 2\times10^5$ we need a small single-atom depumping rate $w_- = N\gamma/1000$ to be in a regime of significant collective effects. The single-atom pumping rate follows as $w_+ = 5w_-$ to create a significant population inversion.

The mean polarization $\langle F_i^0\rangle/F$ along the x-direction strongly depends on the parameter θ as a result of the interplay between the optical pumping along x and quantum jumps described by the collective jump operators $V_i^{\pm}(\theta)$. We can understand this behavior by considering each transition in figure 8(b) involving only two levels and comparing it with

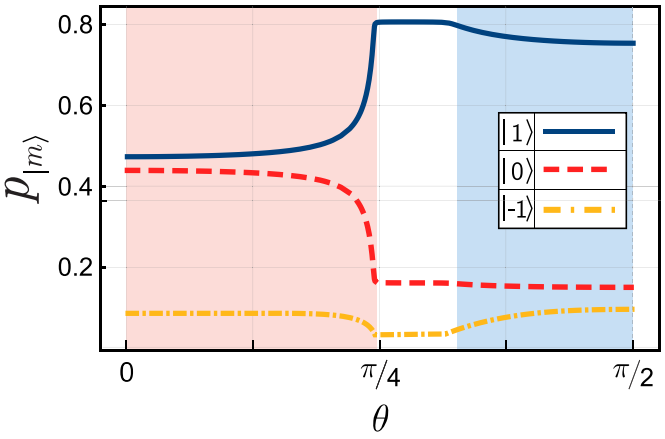

Figure 10. Population $p_{|m\rangle}$ of levels $|m\rangle$ versus θ. Populations experience significant redistribution in the lasing regimes (blue and red shaded areas) as compared to non-lasing regime (white area) where single atom physics prevails. The parameters are the same as in figure 9.

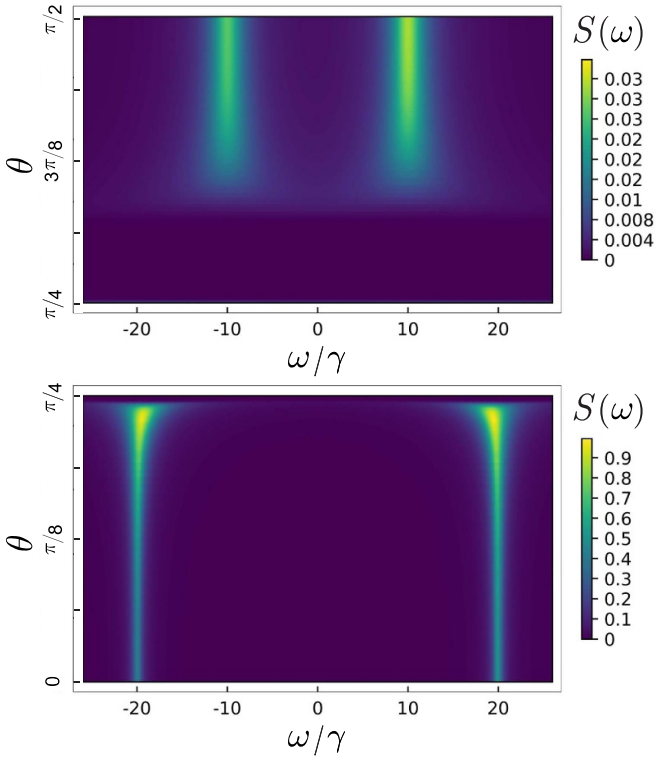

Figure 11. Spectrum $S(\omega)$ of collectively scattered light versus frequency ω on the x-axis and angle θ on the y-axis (separated in two plots due to different color scales). The lower plot shows the two Lorentz peaks at $\omega = \pm 20\gamma$ associated with a superradiant transition on the $0 \leftrightarrow 1$ levels, while the upper plot has the Lorentz peaks at $\omega = \pm 10\gamma$ associated with a superradiant transition on the $-1 \leftrightarrow 0$ levels. The intensity maxima reflect the steady state populations in the respective levels. The parameters are identical to figure 9.

the condition for superradiance (9) of the generalized superradiant laser. For the upper transition $1 \leftrightarrow 0$ and $\theta = 0$ the collective emission with rate $\gamma_{0,1}$ is dominant, due to $\gamma_{0,1}/\gamma_{1,0} = ((2+\epsilon)/(2-\epsilon))^2 > 1$. This allows superradiance, meaning correlations between atoms build up and the atoms emit collectively such that the emitted intensity scales with N^2. For the upper transition and For $\theta > \pi/4$ the collective excitations are dominant, due to $\gamma_{0,1}/\gamma_{1,0} \leqslant 1$, meaning the superradiant condition (9) cannot be fulfilled. Tuning θ between 0 and $\pi/4$ gives a polarization curve in figure 9 similar to figure 6. This similarity is somewhat surprising, as the change of θ in figure 9 entails a *nonlinear* change of the *both* rates $\gamma_{0,1}$, $\gamma_{1,0}$ (see figure 8), while in figure 6 only γ_+ is linearly changed. The lower transition $-1 \leftrightarrow 0$ can fulfill the superradiant condition (9) only for $\theta > \pi/4$, with a maximum dominant collective down rate $\gamma_{-1,0}$ for $\theta = \pi/2$, resulting in a polarization similar to figure 6 with inverted x-axis.

For both, transitions $-1 \leftrightarrow 0$ and $0 \leftrightarrow 1$, superradiance implies an enhanced collective jump rate proportional to N, necessarily decreasing the polarization $\langle F_i^0 \rangle / F$. The superradiant transition in the red shaded region in figure 10 shifts much of the population from $|1\rangle$ to $|0\rangle$, as is shown in figure 10. The small change in population of $|-1\rangle$ is a result of the single-atom depumpings with rate w_- shifting the population of $|0\rangle$ downwards. The superradiant transition in the blue shaded region in figure 10 shifts the population from $|0\rangle$ to $|-1\rangle$. The change in population of $|1\rangle$ is a result of the single-atom depumpings with rate w_- shifting the population of $|1\rangle$ downwards.

The significant θ-dependent redistribution of populations away from the fully polarized state is shown in figure 10. It is also clearly visible that the red shaded regime corresponding to superradiance of the $0 \leftrightarrow 1$ transition involves a much larger population than the blue shaded regime corresponding to superradiance of the $-1 \leftrightarrow 0$ transition. This will be visible also in terms of the intensity of collectively scattered photons.

The spectrum of light collectively scattered to the polarization orthogonal to the laser polarization, $S(\omega) \propto \sum_{i,j=1}^{N} \mathcal{F}[\langle V_i(\tau) V_j(0) \rangle](\omega)$, follows from a Fourier transform of the atomic two-time correlation functions

$$\sum_{i,j=1}^{N} \langle V_i(t+\tau) V_j(t) \rangle = N(N-1) \langle V_2(t+\tau) V_1(t) \rangle + N \langle V_1(t+\tau) V_1(t) \rangle .$$

Here we defined $V_i := V_i^+(\theta) + V_i^-(\theta)$. In order to distinguish contributions from $0 \leftrightarrow 1$ and $-1 \leftrightarrow 0$ transitions in the spectrum we assume a nonlinear Zeeman splitting with, for concreteness, $\omega_{-1} = 0$, $\omega_0 = 10\gamma$, and $\omega_1 = 30\gamma$. This particular level splitting is chosen here such that photons generated on the lower transition occur at a sideband frequency $\omega_0 - \omega_{-1} = 10\gamma$ and for the upper transition at $\omega_1 - \omega_0 = 20\gamma$. The spectrum in figure 11 reveals clearly that for $0 \leqslant \theta < \pi/4$ only the upper transition can be superradiant and for $\pi/4 \leqslant \theta \leqslant \pi/2$ only the lower transition can be superradiant as expected from the superradiant condition (9) and indicated in figure 8(b).

In addition, we extract the full-width at half maximum Γ of the dominant Lorentz peak, as shown in figure 12. In the red and blue shaded superradiant regions, the linewidth Γ is on the same order of magnitude as the collective jump

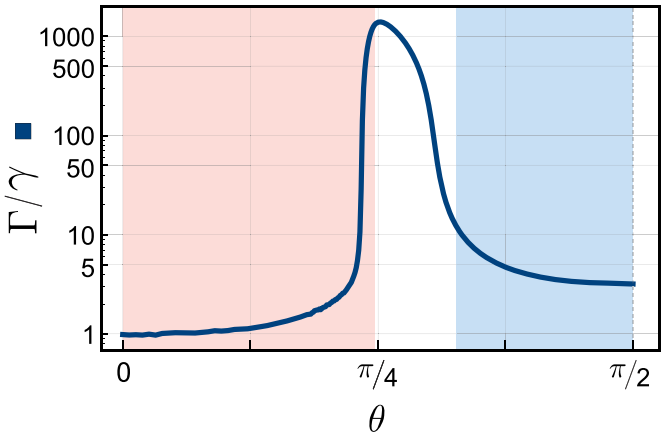

Figure 12. Linewidth (full-width at half maximum) Γ of the highest Lorentz peak versus angle θ. The superradiant regimes (red and blue shaded) show a linewidth on the order of the collective jump rate γ. The parameters are identical to figure 9.

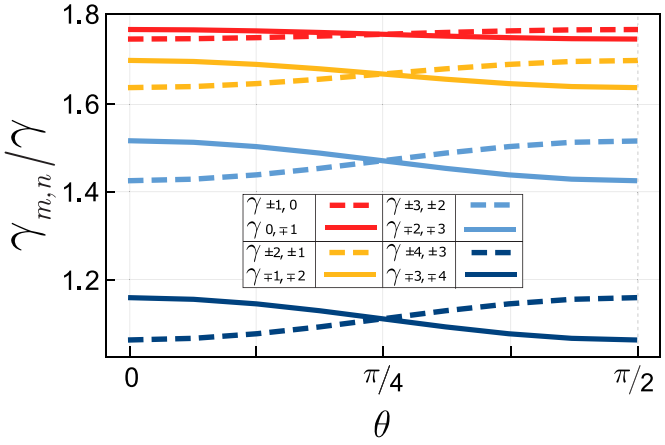

Figure 13. Transition rates $\gamma_{n\pm1,n} = \gamma\langle n \pm 1|V_i^q(\pm\Omega_z)|n\rangle$ (see jump operator (20)) with a Zeeman splitting Ω_z versus the angle θ for $F = 4$ with the parameters given in figure 15. The rates show a similar θ dependence as in the simplified three level model in figure 8, but their absolute value is also dependent on the hyperfine level m.

rate γ. At $\theta = \pi/4$ the dynamics is well approximated by single atom dynamics for which the linewidth is given by $\Gamma = 2\gamma + w_- + w_+$.

3.3. Ground state spin $F = 4$

Finally, we consider as an example the case of the cesium D_2-line with $F = 4$ and $F' = 3, 4, 5$. Here, we consider the complete master equation (18) without any approximation. The steady state is determined as before in cumulant expansion assuming vanishing cumulants of three or more atoms, that is, keeping only two-atom correlations.

Because the full jump operators (23) generate transition rates $\gamma_{n\pm1,n}$ with similar θ dependence (see figure 13), multiple transitions can fulfill the superradiant condition (9) and we expect multiple transitions contributing to the superradiance at the same time. An independent indication of which transitions

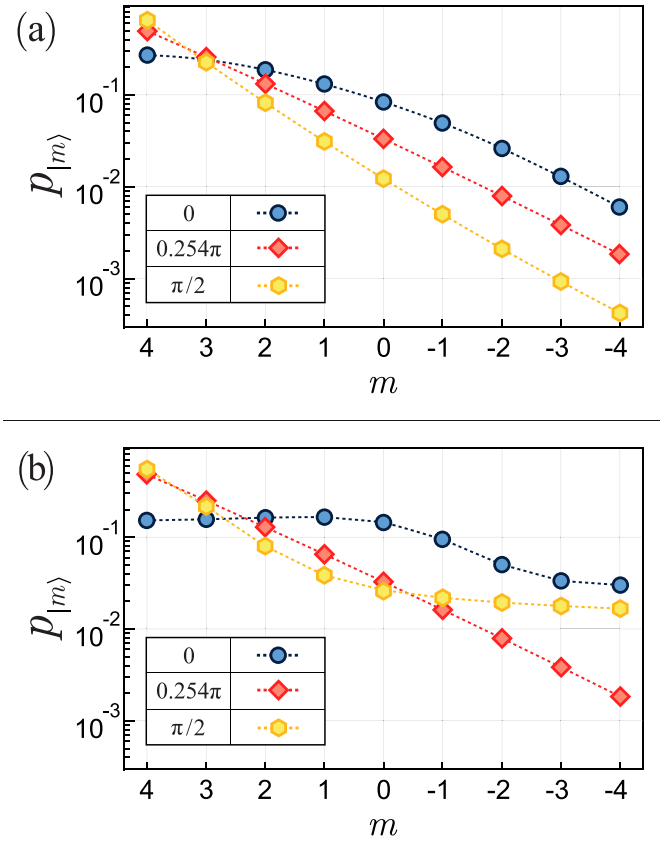

Figure 14. Population $p_{|m\rangle}$ distribution for different angles $\theta = 0, 0.254\pi, \pi/2$ versus the hyperfine levels $|m\rangle$ for the same parameters as in figure 15, figure (a) has optical depth $D \approx 76$ ($N = 2 \times 10^7$ atoms), and (b) optical depth $D \approx 1900$ ($N = 5 \times 10^8$ atoms). The lines connecting the dots are meant as a guide for the eye. (a) and (b) In the non-lasing regime at $\theta = 0.254\pi$, the atoms are uncorrelated and exhibit an exponential distribution of populations, consistent with up and down rates independent on the level m. (b) For $\theta = 0$ the upper transitions become superradiant, meaning also the collective emission rate shifts the population to lower levels canceling the single-atom pumpings and resulting in an almost flat population distribution for $m \geqslant 0$; for $\theta = \pi/2$ the lower transitions are superradiant competing with the single-atom pumpings, giving an almost flat distribution for $m \leqslant 0$. (a) The population for $m \geqslant 0$ is also flattened for $\theta = 0$, but not as pronounced as in (b). For $\theta = \pi/2$ there is no superradiance in any transition and the population remains close to the $\theta = 0.254\pi$ case.

are involved in the superradiance is the population distribution over the different hyperfine levels plotted in figures 14(a) and (b). Figure 14(b) is more instructive to see the pronounced effect of superradiance with optical depth $D \approx 1900$, while figure 14(a) with $D \approx 76$ is more achievable. For uncorrelated atoms around $\theta \approx \pi/4$ the single-atom pumpings dominate, due to the pumping rate w, giving an exponential population distribution in both cases. For $\theta = 0$ figure 14(b) shows the approximately flat distribution for $m \geqslant 0$, indicating that all upper transitions have collective emissions balancing the single-atom pumpings dominantly created by the pumping rate w. This implies that all transitions between levels $m \geqslant 0$ are radiating collectively enhanced, i.e. are superradiant. For $\theta = \pi/2$ one has an inverted behavior in figure 14(b): the population of the upper levels is almost exponential, while the

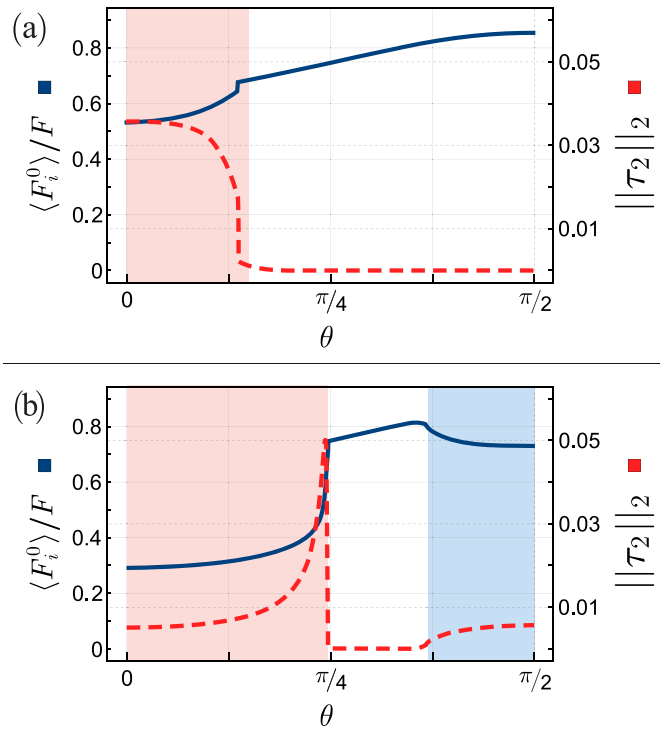

Figure 15. Polarization $\langle F_i^0\rangle/F$, and norm of two-atom correlations $\|\tau_2\|_2$ versus the angle θ for $F=4$, i.e. a nine-level ground state manifold. Figure (a) has optical depth $D\approx 76$ ($N=2\times 10^7$ atoms), and (b) optical depth $D\approx 1900$ ($N=5\times 10^8$ atoms). The two-atom correlations are defined as $\tau_2 := \rho_2-\rho_1\otimes\rho_1$, ρ_n is the reduced density matrix of n atoms, and the red and blue shaded regions correspond to $\|\tau_2\|_2>10^{-3}$. This figure with $F=4$ is the analog to figure 9 in the simplified three-level system. The parameters are the collective jump rate $\gamma/\gamma_{\rm dec}\approx 1.9\times 10^{-6}$, and a pump rate $w/\gamma_{\rm dec}\approx 5.8\times 10^{-3}$. These rates correspond to a laser power $\hbar\omega_c\Phi=6\,$mW, probe beam area $A=(300\,\mu{\rm m})^2$, laser wavelength $\lambda_{\rm L}=852\,$nm, a detuning $\Delta=2\pi\times 3\,$GHz, and pump rate $w=1\,$kHz.

lower levels $m\leqslant 0$ show a flat distribution. In the lower levels the collective emissions are balancing the single-atom pumpings, meaning the transitions between the levels $m\leqslant 0$ are radiating superradiantly. Figure 14(a) shows a less pronounced effect for $\theta=0$ and lacks any superradiance for $\theta=\pi/2$.

Figure 15(b) shows the same qualitative behavior for the polarization and correlations as figure 9 and confirms that the choice of the simplified jump operators (26) captured the dominant effect of the full jump operators (23). The lower optical depth in figure 15(a) compared to figure 15(b) leads to a reduction of the red-shaded θ-range with significant two-atom correlations and prevents any significant two-atom correlations for $\theta>\pi/4$, i.e. no superradiance on any lower transitions.

4. Conclusion

In this article we have used the methods and insights of the superradiant laser [36–38], specifically the self-consistent approximation of the exact dynamics via the cumulant expansion, and applied it to the continuously pumped and off-resonantly probed atomic ensembles as present in experiments such as [24, 30]. In all discussed continuously pumped and probed systems of the article we have seen parameter regimes with steady-states with significant atom–atom correlations strongly influencing observable quantities such as the polarization. This shows that an approximation around the single-atom steady-state, like a simple single-atom mean-field and subsequent Holstein–Primakoff transformation, would have been insufficient to capture these effects.

We see that a self-consistent approximation of the exact dynamics via the cumulant expansion is a suitable way to derive the moment system for spin-1/2 atoms (see sections 2.1 and 2.2) and derive analytical results, such as the superradiant lasing condition (9). For the higher spin atoms the analytical treatment becomes too tedious and one can calculate numerical results as we have shown for the spin-1 atoms in section 3.2 and spin-4 atoms in section 3.3 in a setting of superradiant Raman-lasing.

The key insight in the extension of the superradiant laser in section 2.1 to the generalized superradiant laser in section 2.2 shows strong polarization dependence on the ratio γ_+/γ_- of the collective excitation rate γ_+ and collective emission rate γ_- (see figure 6). This behavior then can be found again in the $F=1$ in figure 9 and $F=4$ in figure 15. Here the x-axis is the linear polarization angle θ of the probe laser, which leads to a change in the collective excitation and collective emission between neighboring excited states (see figures 8 and 13) and has therefore an analog effect on the polarization. This dramatic effect in polarization in continuously pumped and probed atomic ensembles caused by superradiance, meaning collective radiance and resulting atom–atom correlation build-up, should, in principle, be observable in experiments.

Data availability statement

The data that support the findings of this study are available upon reasonable request from the authors.

Acknowledgments

We thank Eugene Polzik and Philipp Treutlein for discussions. K H acknowledges support from Deutsche Forschungsgemeinschaft (DFG, German Research Foundation) under Germany's Excellence Strategy—EXC-2123 QuantumFrontiers—390837967, and Project-ID 274200144—SFB 1227 (DQ-mat, Project A06) through which the results in sections 2.1, 3.1 and 3.3 were obtained. K T acknowledges financial support of the Russian Science Foundation (Project No. 21-72-00049) through which the results in sections 2.2 and 3.2 were obtained.

ORCID iDs

Klemens Hammerer https://orcid.org/0000-0002-7179-0666
Kirill S Tikhonov https://orcid.org/0000-0003-2491-9727

References

[1] Sangouard N, Simon C, de Riedmatten H and Gisin N 2011 *Rev. Mod. Phys.* **83** 33–80
[2] Pezzè L, Smerzi A, Oberthaler M, Schmied R and Treutlein P 2018 *Rev. Mod. Phys.* **90** 035005
[3] Ludlow A D, Boyd M M, Ye J, Peik E and Schmidt P 2015 *Rev. Mod. Phys.* **87** 637–701
[4] Gross C and Bloch I 2017 *Science* **357** 995–1001
[5] Hammerer K, Sørensen A and Polzik E 2010 *Rev. Mod. Phys.* **82** 1041
[6] Deutsch I H and Jessen P S 2010 *Opt. Commun.* **283** 681–94
[7] Kuzmich A, Mandel L and Bigelow N P 2000 *Phys. Rev. Lett.* **85** 1594
[8] Thomsen L K, Mancini S and Wiseman H M 2002 *J. Phys. B: At. Mol. Opt. Phys.* **35** 4937
[9] Smith G A, Chaudhury S and Jessen P S 2003 *J. Opt. B: Quantum Semiclass. Opt.* **5** 323
[10] Smith G A, Chaudhury S, Silberfarb A, Deutsch I H and Jessen P S 2004 *Phys. Rev. Lett.* **93** 163602
[11] Chaudhury S, Smith G A, Schulz K and Jessen P S 2006 *Phys. Rev. Lett.* **96** 043001
[12] Smith G A, Silberfarb A, Deutsch I H and Jessen P S 2006 *Phys. Rev. Lett.* **97** 180403
[13] Inoue R, Tanaka S I R, Namiki R, Sagawa T and Takahashi Y 2013 *Phys. Rev. Lett.* **110** 163602
[14] Hemmer D, Montaño E, Baragiola B Q, Norris L M, Shojaee E, Deutsch I H and Jessen P S 2021 *Phys. Rev.* A **104** 023710
[15] Takano T, Fuyama M, Namiki R and Takahashi Y 2009 *Phys. Rev. Lett.* **102** 033601
[16] Sewell R J, Napolitano M, Behbood N, Colangelo G and Mitchell M W 2013 *Nat. Photon.* **7** 517–20
[17] Behbood N, Colangelo G, Ciurana F M, Napolitano M, Sewell R J and Mitchell M W 2013 *Phys. Rev. Lett.* **111** 103601
[18] Behbood N, Ciurana F M, Colangelo G, Napolitano M, Tóth G, Sewell R and Mitchell M 2014 *Phys. Rev. Lett.* **113** 093601
[19] Julsgaard B, Sherson J, Cirac J I, Fiurášek J and Polzik E S 2004 *Nature* **432** 482–6
[20] Jensen K, Wasilewski W, Krauter H, Fernholz T, Nielsen B M, Owari M, Plenio M B, Serafini A, Wolf M M and Polzik E S 2010 *Nat. Phys.* **7** 13–16
[21] Sherson J F, Krauter H, Olsson R K, Julsgaard B, Hammerer K, Cirac I and Polzik E S 2006 *Nature* **443** 557–60
[22] Krauter H, Salart D, Muschik C A, Petersen J M, Shen H, Fernholz T and Polzik E S 2013 *Nat. Phys.* **9** 400–4
[23] Julsgaard B, Kozhekin A and Polzik E S 2001 *Nature* **413** 400–3
[24] Krauter H, Muschik C A, Jensen K, Wasilewski W, Petersen J M, Cirac J I and Polzik E S 2011 *Phys. Rev. Lett.* **107** 080503
[25] Thomas R A, Parniak M, Østfeldt C, Møller C B, Bærentsen C, Tsaturyan Y, Schliesser A, Appel J, Zeuthen E and Polzik E S 2020 *Nat. Phys.* **17** 228–33
[26] Karg T M, Gouraud B, Ngai C T, Schmid G L, Hammerer K and Treutlein P 2020 *Science* **369** 174–9
[27] Wasilewski W, Jensen K, Krauter H, Renema J J, Balabas M V and Polzik E S 2010 *Phys. Rev. Lett.* **104** 133601
[28] Sewell R, Koschorreck M, Napolitano M, Dubost B, Behbood N and Mitchell M 2012 *Phys. Rev. Lett.* **109** 253605
[29] Koschorreck M, Napolitano M, Dubost B and Mitchell M 2010 *Phys. Rev. Lett.* **105** 093602
[30] Møller C B, Thomas R A, Vasilakis G, Zeuthen E, Tsaturyan Y, Balabas M, Jensen K, Schliesser A, Hammerer K and Polzik E S 2017 *Nature* **547** 191–5
[31] Parkins A S, Solano E and Cirac J I 2006 *Phys. Rev. Lett.* **96** 053602
[32] Muschik C A, Polzik E S and Cirac J I 2011 *Phys. Rev.* A **83** 052312
[33] Huang X, Zeuthen E, Vasilyev D V, He Q, Hammerer K and Polzik E S 2018 *Phys. Rev. Lett.* **121** 103602
[34] Scully M O, Zhu S Y and Gavrielides A 1989 *Phys. Rev. Lett.* **62** 2813
[35] Scully M O, Zhu S Y and Fearn H 1992 *Z. Phys.* D **22** 471–81
[36] Meiser D, Ye J, Carlson D R and Holland M J 2009 *Phys. Rev. Lett.* **102** 163601
[37] Kolobov M, Davidovich L, Giacobino E and Fabre C 1993 *Phys. Rev.* A **47** 1431–46
[38] Bohnet J G, Chen Z, Weiner J M, Meiser D, Holland M J and Thompson J K 2012 *Nature* **484** 78–81
[39] Meiser D and Holland M J 2010 *Phys. Rev.* A **81** 063827
[40] Kirton P and Keeling J 2017 *Phys. Rev. Lett.* **118** 123602
[41] Meiser D and Holland M J 2010 *Phys. Rev.* A **81** 033847
[42] Bohnet J G, Chen Z, Weiner J M, Cox K C and Thompson J K 2013 *Phys. Rev.* A **88** 013826
[43] Xu M, Tieri D, Fine E, Thompson J K and Holland M 2014 *Phys. Rev. Lett.* **113** 154101
[44] Carmichael H J 1991 *An Open Systems Approach to Quantum Optics* (*Lecture Notes*) (Berlin: Springer)
[45] Gardiner C W and Zoller P 2004 *Quantum Noise: A Handbook of Markovian and Non-Markovian Quantum Stochastic Methods with Applications to Quantum Optics* 3rd edn (Berlin: Springer)
[46] Hammerer K 2006 Quantum information processing with atomic ensembles and light *PhD Thesis* Technical University of Munich, Germany
[47] Loudon R 2000 *The Quantum Theory of Light* (*Oxford Science Publications*) 3rd edn (Oxford: Oxford University Press)
[48] Reiter F and Sørensen A S 2012 *Phys. Rev.* A **85** 032111
[49] Breuer H P and Petruccione F 2007 *The Theory of Open Quantum Systems* (Oxford: Oxford University Press)
[50] Geremia J M, Stockton J K and Mabuchi H 2006 *Phys. Rev.* A **73** 042112
[51] Brink D M and Satchler G R 1994 *Angular Momentum* 3rd edn (Oxford: Clarendon)
[52] Roth A 2018 Collective effects and superradiance in atomic ensembles *PhD Thesis* Leibniz University Hannover, Germany
[53] Julsgaard B 2003 Entanglement and quantum interactions with macroscopic gas samples *PhD Thesis* University of Aarhus, Denmark